Multi-Port Network Approach for the Analysis of Dual Band Fractal Microstrip Antennas

Subhrakanta Behera and K. J. Vinoy, *Senior Member, IEEE*

***Abstract*—The multiport network approach is extended to analyze the behavior of microstrip fractal antennas. The capacitively fed microstrip square ring antenna has the side opposite to the feed arm replaced with a fractal Minkowski geometry. Dual frequency operation is achieved by suitably choosing the indentation of this fractal geometry. The width of the two sides adjacent to this is increased to further control the resonant characteristics and the ratio of the two resonance frequencies of this antenna. The impedance matrix for the multiport network model of this antenna is simplified exploiting self-similarity of the geometry with greater accuracy and reduced analysis time. Experimentally validated results confirm utility of the approach in analyzing the input characteristics of similar multi-frequency fractal microstrip antennas with other fractal geometries.**

***Index Terms*—Fractal shaped antenna, microstrip ring antenna, multi-port network model.**

I. Introduction

SEVERAL fractal geometries have been proposed for designing dual frequency, multi-frequency, and wideband antennas in recent years [1]–[6]. Yet the true advantages of using fractals in antennas are widely debated. It remains a fact that the ordered nature of fractals can be exploited in the design and modeling of many such antennas. However, most theoretical analyses so far have been limited to wire or printed fractal antennas such as monopoles or dipoles [1], [6]–[8]. These approaches cannot be easily translated for the analysis of microstrip antennas as the space filling characteristics of underlying fractal geometries are not directly related to the characteristic features of many of these antennas.

A simple approach to analyze irregular shaped microstrip antennas was developed by Professor K.C. Gupta in the 1980s [9]–[13]. This approach starts by decomposing the antenna into regular shaped segments for which the Green's functions can be derived or are readily available. Based on these, network models are developed for each segment. Later these are synthesized to reconstruct the behavior of the original antenna structure [13]. This segmentation approach for the analysis of microstrip antennas was first introduced in [14] for determining the input impedance characteristics of a composite shaped microstrip antennas. The versatility of this approach has been further demonstrated in [15]–[17]. During the last decade this approach has been extended for analyzing microstrip geometries with slots in ground plane [18] and substrate integrated waveguides for millimeter wave applications [19].

In general ring geometries form a class of resonant microstrip antennas in which the mean electrical perimeter determines the resonance frequencies [20]. However due to their high quality factor these geometries especially at their primary resonant modes are seldom used as practical antennas. In addition, the input impedance of these geometries is high when fed directly at a point of symmetry [21]–[25]. However if the energy is electromagnetically coupled into these resonators, their input impedance can be lowered and these are used in practical antenna designs [26]. This group has extended this feed arrangement for multi-frequency antennas by simultaneously exciting multiple rings and dual-frequency antennas with fractal geometries and showed that antennas with reasonable bandwidth can be achieved with this approach [27]–[29].

The proposed antenna has a two layer structure (Fig. 1), in which a ring radiator is placed on the top layer, whereas the feed microstrip transmission line is in a layer beneath this. Although in previous attempts we used an air gap between these dielectric layers, it has been removed here to improve the ease of fabrication [9], [11]. Dielectric substrate (Arlon) with relative dielectric constant of 2.5, loss tangent of 0.0023, and thickness of 1.56 mm is used in this design.

It has been shown that fractal modification to sides of a ring antenna of this type results in dual-frequency antennas. However it is difficult, if not impossible, to replace the wide sides of the ring with fractal geometry. Therefore, in the present study we propose an antenna in which only one side of the square ring is replaced by a fractal geometry (e.g., Minkowski curve of first or second iteration).

For the iterative construction of a fractal Minkowski curve, one starts with the straight line of length l, called the initiator. This is divided into three equal parts of length ($l/3$) and middle segment is replaced by two horizontal and a vertical segment of equal length (Fig. 1(b)). This procedure may be iterated recursively to result in a self similar fractal geometry. In the present study, an antenna design flexibility is introduced by making the length of this vertical segment in Fig. 1(b) vary relative to that of the horizontal segments. Based on this modification, the aspect ratio for the generator is defined as

$$\text{aspect ratio } k = \frac{\text{indentation depth}}{\text{length of segment}}.$$

Manuscript received August 20, 2011; revised March 12, 2012; accepted July 02, 2012. Date of publication July 11, 2012; date of current version October 26, 2012.

S. Behera was with the Microwave Laboratory, Department of Electrical Communication Engineering, Indian Institute of Science, Bangalore 560 012, India. He is now with the School of Electronics Engineering, KIIT University, Bhubaneswar-751024, India (e-mail: subhrajsp@gmail.com).

K. J. Vinoy is with the Microwave Laboratory, Department of Electrical Communication Engineering, Indian Institute of Science, Bangalore 560 012, India (e-mail: kjvinoy@ieee.org).

Color versions of one or more of the figures in this paper are available online at http://ieeexplore.ieee.org.

Digital Object Identifier 10.1109/TAP.2012.2208085

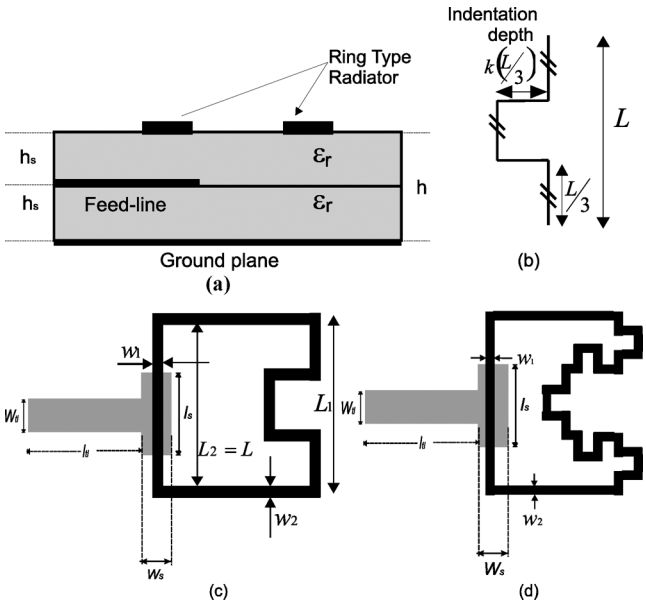

Fig. 1. Geometry of the basic antenna. (a) Cross section view. (b) Minkowski curve generator. (c) Antenna with 1st iteration fractal. (d) Antenna with 2nd iteration fractal.

This aspect ratio is maintained at higher iterations during the generation of the geometry. Similar variation is typically exploited in the context of fractal geometries, the resulting configurations are considered fractals and approaches are available for calculating their fractal properties [1]–[4]. Furthermore, although the most of the theoretical analyses consider the geometry as line segments having zero width, for the sake of realizing antennas, we used geometries with a width of 1.0 mm. This has effectively limited the maximum iteration possible. Top view of the resulting antenna geometries with first and second iteration Minkowski Curve geometries are shown in Fig. 1(c, d).

In this paper we demonstrate the use of multi-port network model based on coplanar Green's functions to analyze the dual frequency behavior of these microstrip ring antennas with fractal segments. Impedance matrices are developed using multi-port network models in Section II for antenna geometries having first and second iteration fractal Minkowski curves. The symmetry of the geometry and the self-similarity properties of fractals have been exploited to reduce the computations involved. The input characteristics obtained by this approach are compared with full wave simulations and experimental results in Section III. Concluding remarks from this study are presented in the last Section.

II. Multi-Port Network Analysis

The antenna under study has a number of small sections which makes the overall geometry quite irregular. It can be expected that the input impedance of the antenna will be affected by the number and locations of corner discontinuities present. Analytical approaches such as cavity model for regular patch geometries are also not suitable in these cases. Hence we propose to use the coplanar multiport network model (MNM) with segmentation approach for the analysis of such fractal antennas. This is a generalization of cavity model, which is suitable for irregular geometries [13]. It may be recalled that the models presented in [3], [7] and [8] are for printed or wire-type dipole and monopole antennas which do not have a ground plane parallel to the geometry. The proposed approach is therefore the first attempt to analyze a fractal microstrip antenna with the geometry parallel to a metallic ground conductor.

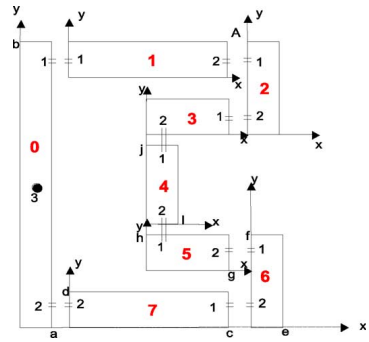

Fig. 2. Segmentation of Square ring microstrip antenna with one side replaced by fractal geometry at first iteration.

In multi-port network approach, the antenna is first decomposed into regular elemental segments that are interconnected using multiple ports. These elemental units are chosen such that Green's functions can be easily computed to evaluate the self and mutual impedance between their ports. Network models of each of these segments are developed using these Greens functions and ports are combined by network synthesis to analyze the behavior of the complete fractal antenna structure [6]. Such segmentation approach was introduced decades ago [14] but several improvisations are required for accurate analysis of irregular antennas with small constitutive segments:

A. Model for Antenna With First Iteration Fractal

In Fig. 1(c) the antenna geometry with the first iteration fractal Minkowski curve is shown. This may be divided into 8 rectangular segments (numbered 0–7) which are interconnected through ports whose locations are marked by two parallel lines in Fig. 2. The 0th segment has an additional incident port. Therefore there are 17 ports in the fragmented geometry. The impedance is evaluated using the voltages, currents at ports of segments. In the following, the voltage, current and impedance of port p of segment s can be written as V_{s_p}, I_{s_p} and Z_{s_p} respectively.

The self and mutual impedances for these segments are computed using Green's function $G(x_i, y_i \,|x_j, y_j)$ [13], [14]. The general formula for the impedance is [12], [30], [31]

$$Z_{n_{ij}} = \frac{1}{w_i w_j} \int_{w_i} \int_{w_j} G(x_i, y_i \,|x_j, y_j)\, dr_i\, dr_j \qquad (1)$$

where the points $(x_i,\ y_i)$ and $(x_j,\ y_j)$ denote the coordinate locations of ports i and j. The integrant dr_i and dr_j are incremental distances over the port width, with the constraint that $w_{i,j} \ll \lambda$ where λ is the wavelength. Hence multiple ports are required to model wide interconnects.

Accurate model for each segment is developed by replacing the fringing fields at the peripheries of the segment geometry by equivalent outward extensions to represent magnetic walls. This

extension Δ depends on shape and planar dimensions of the segment and dielectric constant and thickness of the substrate. The electrical size of the segment is extended marginally to account for fringing. These modified dimensions are used in the evaluation of the above Green's functions. Efficient expressions are available for mutual impedance of rectangular geometries [30], [31]

$$Z_{n_{ij}} = \frac{j\omega\mu h}{b w_i w_j}\left[\frac{w_i w_j}{\mathrm{k}\,\sin\,\mathrm{k}a} - \frac{2ab^2}{\pi^2} \times \sum_{r=1}^{\infty} \frac{(\sin r\theta_1 - \sin r\theta_2)\,(\sin\, r\theta_3 - \sin\, r\theta_4)}{D \sinh D\pi}\right]. \quad (2)$$

The self-impedances of all ports are given by [31]

$$Z_{n_{ii}} = j\omega\mu h\Bigg\{ - \frac{\cos a\mathrm{k} + \cos \mathrm{k}\,(a - 2x_i)}{2b\mathrm{k}\,\sin a\mathrm{k}} + \frac{b^2}{w_i^2\pi^3}\sum_{r=1}^{\infty}\frac{\cosh\frac{a\pi}{b}\sqrt{r^2 - B^2} + \cosh\frac{(a-2x_i)\pi}{b}\sqrt{r^2 - B^2}}{r^2\sqrt{r^2 - B^2}\,\sinh\frac{a\pi}{b}\sqrt{r^2 - B^2}}\Bigg\}. \quad (3)$$

Where a is the length and b is the width of the segments, k is the wave number, $B = b\mathrm{k}/\pi$, $D^2 = (n^2 - B^2)a^2/b^2$, $\theta_1 = (\pi/b)(y_i - w_i/2)$, $\theta_2 = (\pi/b)(y_i + w_i/2)$, $\theta_3 = (\pi/b)(y_j - w_j/2)$, $\theta_4 = (\pi/b)(y_i + w_j/2)$.

Using the impedance values, the voltage and current at the ports of each segment ($n = 1$ to 7) of the geometry in Fig. 2 can be written in general form

$$V_{n_1} = Z_{n_{11}} I_{n_1} + Z_{n_{12}} I_{n_2} \quad (4)$$

$$V_{n_2} = Z_{n_{22}} I_{n_2} + Z_{n_{21}} I_{n_1}. \quad (5)$$

Alternately (4) and (5) may be rewritten as

$$\begin{pmatrix} V_{n_1} \\ V_{n_2} \end{pmatrix} = \begin{pmatrix} Z_{n_{11}} & Z_{n_{12}} \\ Z_{n_{21}} & Z_{n_{22}} \end{pmatrix} \begin{pmatrix} I_{n_1} \\ I_{n_2} \end{pmatrix} \quad \text{or} \quad \boldsymbol{V_n} = \boldsymbol{Z_n I_n} \quad (6)$$

where $\mathbf{Z}_n$ is the impedance matrix for the n^{th} segment. There are 3 ports attached to the input segment (n = 0) and hence the impedance matrix $\mathbf{Z_0}$ is a 3×3 matrix. Therefore, when we include the excitation port (marked as port 3 in Segment 0), there are a total of 17 ports in this geometry and we have 17 voltages and currents to be solved.

However the boundary/continuity conditions can be imposed to reduce the number of unknowns. For example, the voltages and currents at the point marked "A" between segments 1 and 2 of the Fig. 2 are related as

$$V_{1_2} = V_{2_1}, \quad I_{1_2} = -I_{2_1}. \quad (7)$$

Hence these could be generalized for segments number 1 to 6 as

$$V_{n_2} = V_{(n+1)_1},\ I_{n_2} = -I_{(n+1)_1}. \quad (8)$$

For the segment with the excitation port ($n = 0$), the voltages and currents at the interconnection ports are related by

$$V_{0_1} = V_{1_1},\ V_{0_2} = V_{7_2},\ I_{0_1} = -I_{1_1} \ \text{ and } \ -I_{0_2} = I_{7_2}.$$

Furthermore, we can make use of the additional information that the port 3 is located at the middle of the segment, so that the entire geometry is symmetric about the excitation port. Therefore

$$V_{0_1} = V_{0_2},\ I_{0_1} = -I_{0_2}. \quad (9)$$

This may be extended to other interconnecting ports as well. i.e.,

$$V_{n_1} = V_{(8-n)_2},\ I_{n_1} = -I_{(8-n)_2}. \quad (10)$$

Connections between segments are appropriately used to combine these matrices to yield an overall Z-matrix for the given geometry. The seventeen equations can be written in the matrix form as

$$\begin{bmatrix} V_{0_1} \\ V_{0_2} \\ V_{0_3} \\ V_{1_1} \\ V_{1_2} \\ V_{2_1} \\ V_{2_2} \\ - \\ - \\ V_{7_1} \\ V_{7_2} \end{bmatrix} = \begin{bmatrix} Z_{0_{11}} & Z_{0_{12}} & Z_{0_{13}} & 0 & 0 & 0 & 0 & 0 & 0 & 0 & 0 \\ Z_{0_{21}} & Z_{0_{22}} & Z_{0_{23}} & 0 & 0 & 0 & 0 & 0 & 0 & 0 & 0 \\ Z_{0_{31}} & Z_{0_{32}} & Z_{0_{33}} & 0 & 0 & 0 & 0 & 0 & 0 & 0 & 0 \\ 0 & 0 & 0 & Z_{1_{11}} & Z_{1_{12}} & 0 & 0 & 0 & 0 & 0 & 0 \\ 0 & 0 & 0 & Z_{1_{21}} & Z_{1_{22}} & 0 & 0 & 0 & 0 & 0 & 0 \\ 0 & 0 & 0 & 0 & 0 & Z_{2_{11}} & Z_{2_{12}} & 0 & 0 & 0 & 0 \\ 0 & 0 & 0 & 0 & 0 & Z_{2_{21}} & Z_{2_{22}} & 0 & 0 & 0 & 0 \\ - & - & - & - & - & - & - & - & - & - & - \\ - & - & - & - & - & - & - & - & - & - & - \\ 0 & 0 & 0 & 0 & 0 & 0 & 0 & 0 & 0 & Z_{7_{11}} & Z_{7_{12}} \\ 0 & 0 & 0 & 0 & 0 & 0 & 0 & 0 & 0 & Z_{7_{21}} & Z_{7_{22}} \end{bmatrix} \begin{bmatrix} I_{0_1} \\ I_{0_2} \\ I_{0_3} \\ I_{1_1} \\ I_{1_2} \\ I_{2_1} \\ I_{2_2} \\ - \\ - \\ I_{7_1} \\ I_{7_2} \end{bmatrix}. \quad (11)$$

This may be solved to obtain the driving point impedance at port 3 of segment 0 as [13]

$$Z_{in} = \frac{V_{0_3}}{I_{0_3}} = Z_{0_{33}} - \begin{bmatrix} Z_{0_{31}} & Z_{0_{32}} \end{bmatrix} [\mathbf{M}_3]^{-1} \begin{bmatrix} Z_{0_{13}} \\ Z_{0_{23}} \end{bmatrix}. \quad (12)$$

Where the impedance matrix $\mathbf{M}_3$ can be obtained in terms of $\mathbf{M}_3$, $\mathbf{M}_2$ and eventually $\mathbf{M}_1$ which will be related to various port impedances as

$$\mathbf{M}_3 = \begin{bmatrix} Z_{0_{11}} + Z_{1_{11}} & Z_{0_{12}} \\ Z_{0_{12}} & Z_{0_{11}} + Z_{1_{11}} \end{bmatrix} - \begin{bmatrix} Z_{1_{12}} & 0 \\ 0 & Z_{1_{12}} \end{bmatrix} [\mathbf{M}_2]^{-1} \begin{bmatrix} Z_{1_{12}} & 0 \\ 0 & Z_{1_{12}} \end{bmatrix} \quad (13)$$

$$\mathbf{M}_2 = \begin{bmatrix} Z_{1_{11}} + Z_{2_{11}} & 0 \\ 0 & Z_{1_{11}} + Z_{2_{11}} \end{bmatrix} - \begin{bmatrix} Z_{2_{12}} & 0 \\ 0 & Z_{2_{12}} \end{bmatrix} [\mathbf{M}_1]^{-1} \begin{bmatrix} Z_{2_{12}} & 0 \\ 0 & Z_{2_{12}} \end{bmatrix} \quad (14)$$

$$\mathbf{M}_1 = \begin{bmatrix} Z_{2_{11}} + Z_{3_{11}} & 0 \\ 0 & Z_{2_{11}} + Z_{3_{11}} \end{bmatrix} - \begin{bmatrix} Z_{3_{12}} & 0 \\ 0 & Z_{3_{12}} \end{bmatrix} \cdot \begin{bmatrix} Z_{3_{22}} + Z_{4_{11}} & Z_{4_{12}} \\ Z_{4_{12}} & Z_{3_{22}} + Z_{4_{11}} \end{bmatrix}^{-1} \begin{bmatrix} Z_{3_{12}} & 0 \\ 0 & Z_{3_{12}} \end{bmatrix}. \quad (15)$$

The losses (primarily by radiation) from the antenna can be incorporated into these expressions by modifying k in (2) and (3) [32]

$$k = \sqrt{\omega^2 \mu \varepsilon_0 \varepsilon_{eff} \left(1 - \frac{j}{Q}\right)}. \quad (16)$$

where Q is the total quality factor of the resonating antenna. When we consider more than one resonance for an antenna, the Q may be different at these frequencies.

Another important aspect to notice is that the input impedance given by (12) is for a port physically connected to the segment 0 at the location of port 3 there. However, the antenna configuration in Fig. 1 consists of an electromagnetic coupling using a capacitive strip placed symmetrically below the ring resonator. The input impedance of the antenna appears in series with this coupling impedance as

$$Z_{ant} = (Z_{pp} + Z_{in}) \times g \quad (17)$$

where g, is the critical electromagnetic coupling to the antenna and Z_{pp} is the impedance of the parallel plate capacitor section

$$Z_{pp} = \frac{h_s}{j\omega \varepsilon_r \varepsilon_0 A_f} \quad (18)$$

where h_s is the substrate height and A_f is the overlap area of the simple parallel plate capacitor between the feed strip and the radiating patch.

B. Model for the Second Iteration

The multi-port network model with segmentation approach described above can be easily extended for antenna geometry with the second iteration fractal geometry. The primary difference in this case is that there are 28 segments to be considered. These are marked 0 to through 27 in Fig. 3. The coupling impedances and self impedances in each case can be evaluated by following the above approach. The resulting equations can be solved and reduced to a single resultant equation similar to (12).

The resulting impedance matrix can be further simplified making use of similarity between various sections of geometry. Some of these repeated segments as indicated by ovals in Fig. 3. One can easily verify the following impedance matrices to be equal

$$\mathbf{Z}_3 = \mathbf{Z}_5 = \mathbf{Z}_7 = \mathbf{Z}_{13},\ \mathbf{Z}_4 = \mathbf{Z}_{14},\ \mathbf{Z}_8 = \mathbf{Z}_{10} = \mathbf{Z}_{12}. \quad (19)$$

These simplify the number of terms to be computed for the final matrix equation relating voltages and currents. Thus this approach exploits the self-similarity of fractal geometries.

These expressions are used to compute the S_{11} of the antenna with the second iteration geometry. It may be noted that computation of many redundant terms in the impedance matrix may be avoided based on the symmetry and self-similarity of the geometry. Another important aspect of this approach is that this may be extended to many other fractal shaped planar antenna geometries. For example, modified Sierpinski gasket [2] and Sierpinski carpet [33] geometries used in these antennas may be modeled by this approach.

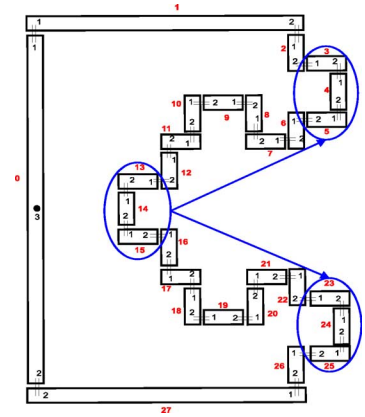

Fig. 3. Segmentation of Square ring microstrip antenna with one side replaced by the second iteration fractal geometry.

III. Validation and Discussion

It may be noted from the previous discussions that in this approach the irregular-shaped fractal antenna geometry is divided into various segments which themselves have simpler shapes and each segment is considered as a multiport section with a finite number of ports. The number of ports required at an intersection between two segments is determined by the width of the interconnection. The multiport Z-matrices for individual segments are evaluated using the corresponding impedance Green's functions. The interconnection constraints are applied by the continuity of the voltage and currents at the boundaries between segments.

One of the important features of this approach is that the computation of elements in the overall Z-matrix can be simplified making use of the symmetry if any, of the overall geometry. Using this simplified Z-matrix, the driving point impedance at the input port of the antenna can be evaluated.

Models developed in Section II are validated by simulations and experiments. Dielectric substrate (Arlon) with relative dielectric constant of 2.5, loss tangent of 0.0023, and thickness of 1.56 mm is used to develop experimental prototypes.

A. Validation by Simulations

These antenna geometries were studied extensively by IE3D simulations. An increase in the indentation depth causes the perimeter of the antenna to increase and hence the resonance frequencies shift downward. The calculated resonance frequencies are compared well with simulations of the given antenna of varying indentation factor as shown in Tables I and II.

For patches of arbitrary shapes can be analyzed by MNM model by treating the arbitrary shapes as a combination of the elementary shapes for which Green's functions are available. Since, most of the elements of the fractal shape patch antenna are similar and repeatable due to the recursive nature of the

TABLE I
VALIDATION WITH SIMULATED RESULTS FOR THE FRACTAL ANTENNA SHOWN IN FIG. 1(d) FOR A VARIATION IN THE INDENTATION DEPTH. OTHER DESIGN PARAMETERS ARE $W_1 = 1$ mm, $W_2 = 3$ mm, $L_1 = 25.7$ mm, $L_2 = 19.7$ mm

Indentation factor *(k)*	First resonance		Second resonance	
	f_{r1} (GHz.) Simulated.	f_{r1} (GHz.) Calculated.	f_{r2} (GHz.) Simulated.	f_{r2} (GHz.) Calculated.
0.8	2.4	2.402	4.25	4.252
0.9	2.336	2.333	4.12	4.118
1	2.274	2.275	3.991	3.988
1.1	2.211	2.2	3.872	3.871
1.2	2.148	2.152	3.76	3.755

TABLE II
VALIDATION WITH SIMULATED RESULTS FOR THE FRACTAL ANTENNA SHOWN IN FIG. 1(d) FOR A VARIATION IN THE INDENTATION DEPTH. OTHER DESIGN PARAMETERS ARE $W_1 = 1$ mm, $W_2 = 7$ mm, $L_1 = 29.7$ mm, $L_2 = 15.7$ mm

Indentation factor *(k)*	First resonance		Second resonance	
	f_{r1} (GHz.) Simulated.	f_{r1} (GHz.) Calculated.	f_{r2} (GHz.) Simulated.	f_{r2} (GHz.) Calculated.
0.8	2.842	2.839	4.54	4.542
0.9	2.785	2.785	4.4	4.401
1	2.725	2.723	4.275	4.279
1.1	2.66	2.67	4.16	4.161
1.2	2.596	2.595	4.05	4.051

fractal, so the computation time will reduce significantly by using this analysis technique with improved accuracy

It may be noted from Tables I and II that the resonance frequency calculated using multi-port network model compared well with the simulations. It may be seen that the percentage error is 0.08 – 1.86% at the first resonance frequency and 0.05 – 1.01% at the second resonance frequency, for the cases considered in these tables. But the resonance frequency of these antennas calculated using lossy transmission line (LTL) model [24], [25] does not compare well with the simulations. For example, if LTL is employed the error is 7 – 13% at the first resonance frequency and 11 – 18% at the second resonance frequency. This is because the LTL model considers only the physical straightened length and not the mutual coupling between parts of the geometry, causing the computed resonance frequencies to be lower than those obtained from simulations. But in the case of multi-port network model, the self-impedances and the mutual impedances of adjacent elements are computed and therefore this approach performs better than LTL model for this type of geometries.

It may be noted that, for the geometries studied here, the ratios of resonance frequencies vary between 1.56 and 2.017. These results indicate that the use of fractal Minkowski geometry in these antenna configurations can result in useful dual frequency antenna. Another interesting characteristic of this antenna geometry is that the bandwidth of non-uniform width antenna is often higher than a uniform width ring antenna of similar dimensions.

B. Validation by Experiments

The fabricated antennas are shown in Fig. 4. This antenna has a non-uniform width ring having $w_1 = 1$ mm, $w_2 = 7$ mm, the length of the initiator $= 15.7$ mm and the indentation factor $= 1$. The antenna is excited through electromagnetic coupling from a transmission line buried in a dielectric layer beneath. An aluminum ground plane of dimensions 20 cm × 20 cm supports this structure. The transmission line is fed using a probe-type SMA connector. The fabricated antennas are tested using a vector network analyzer.

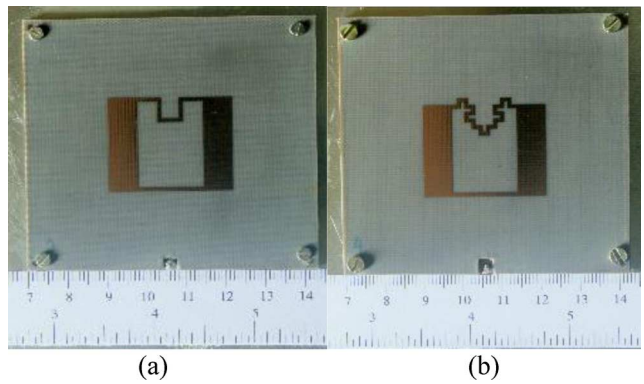

Fig. 4. Photographs of fabricated antennas.

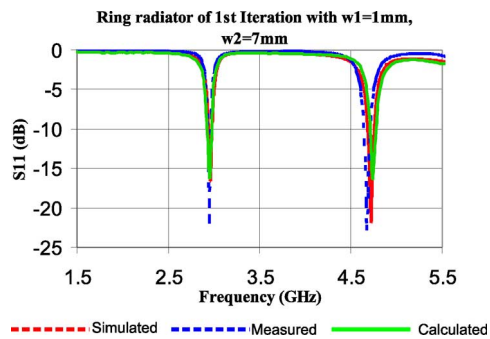

Fig. 5. Comparison of return loss characteristics of antenna shown in Fig. 4(a).

The measured return loss characteristics of the antenna with the first iteration geometry are compared with analytical calculations and numerical simulations in Fig. 5. Analytical plots are obtained using the formulation from Section II whereas the simulated one is obtained using IE3D method of moment based simulations. These results clearly validate the approach for the calculation of antenna impedance. This graph also shows that the bandwidths at the two resonance frequencies are as expected. For the calculations the value of Q used are 54.8938 and 47.3751 and the coupling coefficient values are 0.0211 and 0.0290 at the two resonance frequencies of the antenna.

Measured radiation patterns (Fig. 6) at these frequencies indicate that these have similar radiation patterns at both bands. The gain of the antenna in the boresight direction has been measured to be 5.2 dBi and 4.5 dBi respectively at the corresponding resonance frequencies.

Similarly, for the second iteration geometry shown in Fig. 4(b) is studied through Figs. 7 and 8. In this case, the coupling coefficients used are 0.0028 and 0.20 and the quality factors are 66.0112 and 50.573 at its resonance frequencies. The

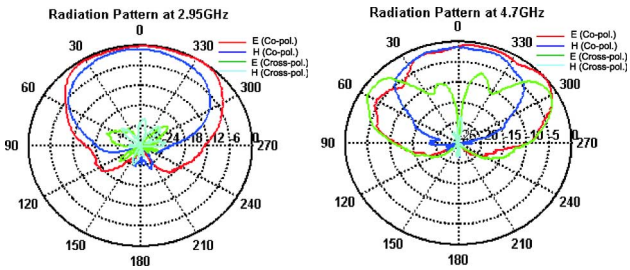

Fig. 6. Measured radiation patterns at first and second resonance frequencies of the antenna shown in Fig. 4(a).

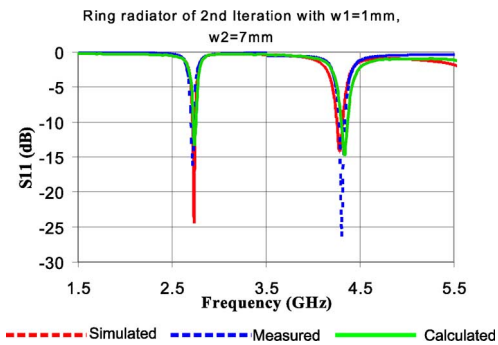

Fig. 7. Comparison of return loss characteristics of Square ring microstrip antenna shown in Fig. 4(b).

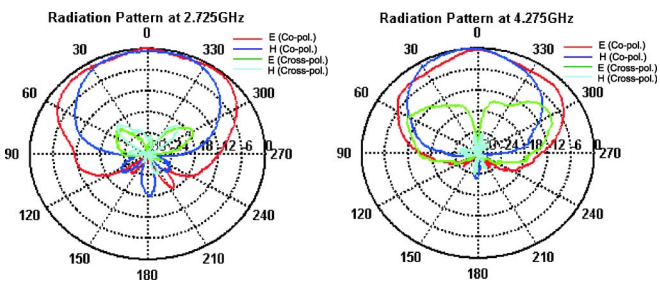

Fig. 8. Measured radiation patterns at first and second resonance frequencies of antenna shown in Fig. 4(b).

radiation patterns of this antenna at the resonance frequencies are similar to those in Fig. 6.

A summary of the performance of these fractal antennas is presented in Table III. These reiterate that this fractal antenna has dual frequency characteristics with reasonable gain and bandwidth at both resonances. The reasons behind the dual frequency nature of similar antennas have been discussed previously [28], [29]. When fractal segments replaces the straight section of the square ring, the overall symmetry of the antenna is displaced, and the currents distribution changes. By suitably choosing the indentation factor the gain in the boresight direction at second resonance can therefore be made equal to that at the first resonance. When the width of two segments are increased, the current paths at the inner and outer edges of these segments are perturbed causing the bandwidth and radiation efficiency to increase.

TABLE III
COMPARISON OF THE SIMULATED AND MEASURED PERFORMANCES OF THE DUAL-FREQUENCY MICROSTRIP RING ANTENNAS. THE DIMENSIONS OF FEED STRIP (L_S, W_S) HAS BEEN OPTIMIZED FOR A GOOD IMPEDANCE MATCH FOR THE ANTENNA

Antenna Model	1st iteration Geometry w1=1mm,w2=7mm (Fig. 6a)		2nd iteration Geometry w1=1mm,w2=7mm (Fig. 6 b)	
	f_{r1}	f_{r2}	f_{r1}	f_{r2}
Simulated Resonance frequency (GHz)	2.95	4.71	2.725	4.275
Measured Resonance frequency (GHz)	2.945	4.75	2.78	4.298
Simulated Bandwidth (MHz)	38	70.3	29.19	59.8
Measured Bandwidth (MHz)	35.05	72.2	28.5	60.8
Simulated Gain (dBi)	5.98	4	5.66	5.3
Measured Gain (dBi)	5.2	4.5	4.45	5.4

IV. CONCLUSIONS

A dual frequency antenna obtained by replacing a segment of a square ring microstrip antenna with fractal Minkowski curve is studied here. It has been observed that by increasing the indentation factor in the fractal section of the radiator, the resonance frequencies of the antenna changes and by suitably choosing this value one can get an antenna design with improved bandwidth with good gain at both the resonance frequencies. Increase in the width of other two sides of the ring significantly enhances its radiation characteristics. The geometry for this dual-frequency antenna may be chosen such that the ratio of resonance frequencies may be controlled by these design parameters. Results presented here also indicate a similar behaviour for the first- and second-iteration fractal geometries.

A multiport network approach is shown to be very effective to analyze this antenna. Developed about four decades ago, this method has been shown to be versatile for analyzing many planar geometries. This approach exploits the ordered nature of fractals in simplifying the analysis, and avoids computation redundancy. The behavior of antennas with the first and second iteration fractal geometries have been accurately modeled with this approach and are validated against simulations using commercial full wave softwares and experimental results.

REFERENCES

[1] K. J. Vinoy, K. A. Jose, and V. K. Varadan, "On the relationship between fractal dimension and the performance of multi-resonant dipole antennas using Koch curves," *IEEE Trans Antennas Propag.*, vol. 51, no. 9, pp. 2296–2303, Sep. 2003.

[2] J. Yeo and R. Mittra, "Modified Sierpinski gasket patch antenna for multiband applications," in *Proc. IEEE Antennas and Propagation Soc. Int. Symp.*, 2001, vol. 3, pp. 134–137.

[3] K. J. Vinoy, K. A. Jose, V. K. Varadan, and V. V. Varadan, "Hilbert curve fractal antenna: A small resonant antenna for VHF/UHF application," *Microw. Opt. Technol. Lett.*, vol. 29, no. 4, May 2001.

[4] Y. B. Thakare and Rajkumar, "Design of fractal patch antenna for size and radar cross-section reduction," *IET Microw., Antennas Propag.*, vol. 4, no. 2, pp. 175–181, Feb. 2010.

[5] J. Pourahmadazar, C. Ghobadi, J. Nourinia, and H. Shirzad, "Multi-band ring fractal monopole antenna for mobile devices," *IEEE Trans. Antennas Wireless Propag. Lett.*, vol. 9, pp. 863–866, 2010.
[6] D. C. Chang, B. H. Zeng, and J. C. Liu, "CPW-fed circular fractal slot antenna design for dual-band applications," *IEEE Trans Antennas Propag.*, vol. 56, no. 12, pp. 3630–3636, Dec. 2008.
[7] M. Comisso, "Theoretical and numerical analysis of the resonant behaviour of the Minkowski fractal dipole antenna," *IET Microw. Antennas Propag.*, vol. 3, no. 3, pp. 456–464, 2009.
[8] K. J. Vinoy, K. A. Jose, and V. K. Varadan, "Impact of fractal dimension in the design of multi-resonant fractal antennas," *Fractals*, vol. 12, pp. 55–66, 2004.
[9] R. Chadha and K. C. Gupta, "Segmentation method using impedance matrices for the analysis of planar microwave circuits," *IEEE Trans. Microw. Theory Tech.*, vol. MTT-29, pp. 71–74, Jan. 1981.
[10] P. C. Sharma and K. C. Gupta, "Desegmentation method for analysis of two-dimensional microwave circuits," *IEEE Trans. Microw. Theory Tech.*, vol. MTT-29, pp. 1094–1098, Oct. 1981.
[11] A. Benalla and K. C. Gupta, "Multiport network approach for modeling the mutual coupling effects in microstrip patch antennas and arrays," *IEEE Trans Antenna Propag.*, vol. 31, no. 2, pp. 148–152, 1989.
[12] A. Benalla and K. C. Gupta, "Faster computation of Z-matrices for rectangular segments in planar microstrip circuits," *IEEE Trans. Microw. Theory Tech.*, vol. MTT-34, no. 6, pp. 733–736, Jun. 1986.
[13] K. C. Gupta, "Multiport network approach for modeling and analysis of patch antennas and arrays," in *Handbook of Microstrip Antennas*, J. R. James and P. S. Hall, Eds. London, U.K.: Peter Peregrinus Ltd., 1989, ch. 9.
[14] T. Okoshi and T. Miyoshi, "The planar circuit-an approach to microwave integrated circuitry," *IEEE Trans Microw. Theory Tech.*, vol. MTT-20, no. 4, Apr. 1972.
[15] R. P. Parrikar and K. C. Gupta, "Multiport network model for CAD of electromagnetically coupled microstrip patch antennas," *IEEE Trans Antenna Propag.*, vol. 46, no. 5, pp. 475–483, May 1998.
[16] A. A. Deshmukh and G. Kumar, "Even-mode multiport network model for slotted dual-band rectangular microstrip antennas," *Microw. Opt. Technol. Lett.*, vol. 48, no. 4, pp. 798–804, Apr. 2006.
[17] A. A. Deshmukh and K. P. Ray, "Stub loaded multi-band slotted rectangular microstrip antennas," *IET Microw., Antennas Propag.*, vol. 3, no. 3, pp. 529–535, Apr. 2009.
[18] A. Khajehnasiri and S. Safavi-Naeini, "A generalized 2-D multiport model for planar circuits with slots in ground plane," *IEEE Trans. Antenna Propag.*, vol. 55, no. 5, pp. 1283–1292, May 2007.
[19] E. Abaei, E. Mehrshahi, and H. R. Sadreazami, "Analysis of substrate integrated waveguide based on two dimensional multi-port method," in *Proc. Int. Conf. Microwave and Millimeter Wave Technology (ICMMT)*, Chengdu, China, May 8–11, 2010, pp. 793–796.
[20] L. H. Hsieh and K. Chang, "Equivalent lumped elements G, L, C, and unloaded Q's of closed- and open-loop ring resonators," *IEEE Trans. Microw. Theory Tech.*, vol. MTT-50, no. 2, pp. 453–460 , Feb. 2002.
[21] J. W. Mink, "Circular ring microstrip antenna elements," in *IEEE AP-S Int. Symp. Digest*, 1980, pp. 605–608.
[22] P. M. Bafrooei and L. Shafai, "Characteristics of single- and double-layer microstrip square-ring antennas," *IEEE Trans. Antennas Propag.*, vol. 47, no. 10, pp. 1633–1639, Oct. 1999.
[23] W. S. Chen, C. K. Wu, and K. L. Wong, "Single-feed Square-ring microstrip antenna with truncated corners for compact circular polarization operation," *Electron. Lett.*, vol. 34, no. 11, May 1998.
[24] I. J. Bahl, S. S. Stuchly, and M. A. Stuchly, "A new macrostrip radiator for medical applications," *IEEE Trans. Microw. Theory Tech.*, vol. MTT-28, no. 12, pp. 1464–1468, Dec. 1980.
[25] R. Garg and V. S. Reddy, "Edge feeding of microstrip ring antennas," *IEEE Trans. Antennas Propag.*, vol. 51, no. 8, pp. 1941–1946, Aug. 2003.
[26] G. Mayhew-Ridgers, J. W. Odendaal, and J. Joubert, "New feeding mechanism for annular-ring microstrip antenna," *Electron. Lett.*, vol. 36, no. 7, Mar. 2000.
[27] A. Pal, S. Behera, and K. J. Vinoy, "Design of multi-frequency microstrip antennas using multiple rings," *IET Microw., Antennas Propag.*, vol. 3, pp. 77–84, 2009.
[28] S. Behera and K. J. Vinoy, "Microstrip square ring antenna for dual-band operation," *Progr. Electromagn. Res.*, vol. PIER 93, pp. 41–56, 2009.
[29] K. J. Vinoy and A. Pal, "Dual-frequency characteristics of Minkowski-square ring antennas," *IET Microw., Antennas Propag.*, vol. 4, no. 2, pp. 219–224, 2010.
[30] E. G. Lim, E. Korolkiewiewicz, S. Scott, B. Aljibouri, and S. C. Gao, "Efficient impedance coupling formulas for rectangular segment in planar microstrip circuits," *IEEE Trans. Antennas Propag.*, vol. 51, no. 8, pp. 2137–2140, Aug. 2003.
[31] S. F. Ooi, S. K. Lee, A. Sambell, E. Korolkiewicz, and S. Scott, "A new and explicit matrix input impedance formula for the H-shaped microstrip patch antenna," *Microw. Opt. Technol. Lett.*, vol. 49, no. 7, Jul. 2007.
[32] D. M. Pozar, *Microwave Engineering*, 2nd ed. New Delhi, India: Wiley, 2003.
[33] W. –L. Chen and G –M. Wang, "Small size edge-fed Sierpinski carpet microstrip patch antennas," *Prog. Electromagn. Res. C*, vol. 3, pp. 195–202, 2008.

Subhrakanta Behera was born in Orissa, India. He received the B.Sc. degree from Utkal University in 1995, the M.Sc. degree from Berhampur University in 1997, the M.Tech. degree from Cochin University of Science and Technology, Kochi, Kerala, in 2004, and the Ph.D. degree from Indian Institute of Science, Bangalore-12, India, in 2011, under the guidance of Prof. K. J. Vinoy.

He spent a year as a Postdoctoral Research Fellow at the GE Global Research Center, Bangalore. He is currently an Assistance Professor in the School of Electronics Engineering, KIIT University, Bhubaneswar, India. His research interest is in the field of computational electromagnetics and microwave engineering.

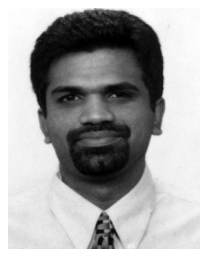

K. J. Vinoy (M'02–SM'06) received the B.Sc. degree from the University of Kerala, Kerala, India, the M.Sc. degree from Cochin University of Science and Technology, Cochin, India, and the Ph.D. degree from the Pennsylvania State University, University Park, in 1990, 1993, and 2002, respectively.

From 1994 to 1998, he worked in various positions at the National Aerospace Laboratories, Bangalore, India, where he was attached to the Computational Electromagnetics Group. He was a Research Assistant at the Center for the Engineering of Electronic and Acoustic Materials and Devices (CEEAMD) at the Pennsylvania State University, from 1999 to 2002. He continued there for Postdoctoral research until 2003. Since 2003, he has been with the Department of Electrical Communication Engineering, Indian Institute of Science, Bangalore, where he is currently an Associate Professor. His research interests cover several aspects of microwave engineering including, microwave antennas, microwave circuits, metamaterials and RF MEMS. He has published over 100 papers in technical journals and conferences. He has also published five books: *Radar Absorbing Materials: From Theory to Design and Characterization* (Kluwer, 1996), *RF MEMS and their Applications* (Wiley, 2002), *Smart Material Systems and MEMS: Design and Development Methodologies* (Wiley, 2006), *Micro and Smart Systems (*New Delhi: John Wiley & Co. 2010), and *Micro and Smart Systems: Technology & Modeling*, (Wiley. 2012). He is serving on the editorial board of the *Journal of the Indian Institute of Science*.

Prof. Vinoy is currently the Chairman of the IEEE joint MTT/AP Societies Bangalore Chapter.